Mode field patterns and preferential mode coupling in planar waveguide-coupled square microcavities

Chung Yan Fong and Andrew W. Poon

Department of Electrical & Electronic Engineering, The Hong Kong University of Science and Technology, Clear Water Bay, Hong Kong SAR, China.
eeawpoon@ust.hk

Abstract: We report a numerical and analytical study of mode field patterns and mode coupling in planar waveguide-coupled square microcavities, using two-dimensional (2-D) finite-difference time-domain (FDTD) method and k-space representation. Simulated mode field patterns can be identified by k-space modes. We observe that different mode number parities permit distinctly different mode field patterns and spectral characteristics. Simulation results suggest that k-space modes that nearly match the waveguide propagation mode have a relatively high coupling efficiency. Such preferential mode coupling can be modified by the mode number parity.

OCIS codes: (230.5750) Resonators; (260.5740) Resonance

References and links

1. D. Rafizadeh, J. P. Zhang, S. C. Hagness, A. Taflove, K. A. Stair, S. T. Ho and R. C. Tiberio, "Waveguide-coupled AlGaAs/GaAs microcavity ring and disk resonators with high finesse and 21.6-nm free spectral range," Opt. Lett. **22**, 1244-1246 (1997).
2. S. C. Hagness, D, Rafizadeh, S. T. Ho and A. Taflove, "FDTD microcavity simulations: design and experimental realization of waveguide-coupled single-mode ring and whispering-gallery-mode disk resonators," J. Lightwave Technol. **15**, 2154-2165 (1997).
3. B. E. Little, J. S. Foresi, G. Steinmeyer, E. R. Thoen, S. T. Chu, H. A. Haus, E. P. Ippen, L. C. Kimerling and W. Greene, "Ultra-compact Si-SiO2 microring resonator optical channel dropping filters," IEEE Photon. Technol. Lett. **10**, 549-551 (1998).
4. D. J. W. Klunder, F. S. Tan, T. van der Veen, H. F. Bulthuis, G. Sengo, B. Docter, H. J. W. M. Hoekstra and A. Driessen, "Experimental and numerical study of SiON microresonators with air and polymer cladding," J. Lightwave Technol. **21**, 1099-1110 (2003).
5. R. Grover, T. A. Ibrahim, T. N. Ding, Y. Leng, L. C. Kuo, S. Kanakaraju, K. Amarnath, L. C. Calhoun and P. T. Ho, "Laterally coupled InP-based single-mode microracetrack notch filter," IEEE Photon. Technol. Lett. **15**, 1082-1084(2003).
6. C. Manolatou, M. J. Khan, S. Fan, P. R. Villeneuve, H. A. Haus and J. D. Joannopoulos, "Coupling of modes analysis of resonant channel add-drop filters," IEEE J. Quantum Electron. **35**, 1322-1331 (1999).
7. A. W. Poon, F. Courvoisier and R. K. Chang, "Multimode resonances in square-shaped optical microcavities," Opt. Lett. **26**, 632-634 (2001).
8. A. W. Poon, "Optical resonances of two-dimensional microcavities with circular and non-circular shapes," PhD thesis, Yale University, 2001.
9. Y. L. Pan and R. K. Chang, "Highly efficient prism coupling to whispering gallery modes of a square μ cavity," Appl. Phys. Lett. **82**, 487-489 (2003).
10. M. Lohmeyer, "Mode expansion of rectangular integrated optical microresonators," Opt. Quantum Electron. **34**, 541-557 (2002).
11. M. Hammer, "Resonant coupling of dielectric optical waveguides via rectangular microcavities: the coupled guided mode perspective," Opt. Commun. **214**, 155-170 (2002).
12. Y. F. Chen, K. F. Huang, H. C. Lai and Y. P. Lan, "Observation of vector vortex lattices in polarization states of an isotropic microcavity laser," Phys. Rev. Lett. **90**, 053904 (2003).
13. N. Ma, C. Y. Fong, F. K. L. Tung, K. C. Lam, W. N. Chan and A. W. Poon, "Micro-pillar square resonant cavity channel add-drop filters on silicon-nitride-on-silica: design, fabrication and characterization," in Proc. of Conf. Lasers Electro-Optics, Baltimore, MD, Jun. 2003.

#3001 - $15.00 US Received September 04, 2003; Revised October 24, 2003

14. FullWAVE, Rsoft Inc. Research Software, http://www.rsoftinc.com.
15. K. Okamoto, "Chapter 2" in *Fundamentals of optical waveguides*, (Academic, San Diego, CA, 2000).

1. Introduction

Planar waveguide-coupled microcavities (μ-cavities) in the form of circular ring and disk [1-4], racetrack [5], and square [6,10,11,13] have been attracting considerable interest for channel add-drop applications in wavelength-division multiplexed (WDM) networks. Lightwave can be partially confined by total internal reflection (TIR) at the μ-cavity sidewalls, so that optical resonances can be excited when the cavity round-trip lightwave is wavefront-matched with the input-coupled lightwave. The shortcoming of the conventional circular μ-cavities is that the short interaction length between the curved cavity sidewall and the laterally coupled straight waveguides imposes sub-micrometer air-gap spacing for evanescent coupling. Recently, a number of research groups have proposed square μ–cavities that have high-Q resonances and long interaction length along the entire flat cavity sidewalls as an alternative resonator to ease the air-gap spacing tolerance [6-11,13]. Multimodes of square μ–cavities, which are attributed to k-space modes of the cavity with mirror-like boundaries [7,8], have been experimentally demonstrated by Gaussian beam coupling [7,8] and by prism coupling [9].

Planar waveguide-coupled square and rectangular μ–cavities have also been investigated analytically using coupled mode theory by modeling the cavity as a singlemode standing wave resonator [6] and directional coupler segment [11], and numerically by finite-difference time-domain (FDTD) [6] and mode expansion method [10,11]. In this paper, we, on the other hand, consider square μ–cavities as multimode resonators. We model and analyze (i) the multimode resonances of square μ–cavities and (ii) the mode coupling between the square μ–cavity and the laterally coupled waveguides. Multimode spectra and mode field patterns of planar waveguide-coupled square μ-cavity channel add-drop filters are numerically simulated using two-dimensional (2-D) FDTD method. We interpret the FDTD results by means of k-space modes of a discrete square μ–cavity with mirror-like boundaries [7]. Simulated mode field patterns can be modeled by the interference of degenerate pairs of k-space modes. Simulation results show that k-space modes that nearly match the waveguide modes can in general be preferentially input-coupled.

2. Planar waveguide-coupled square μ-cavities

2.1 k-space modes of discrete square cavities

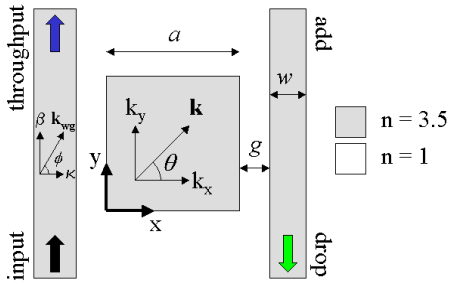

Fig. 1. Schematic of a planar waveguide-coupled square μ-cavity channel add-drop filter.

Figure 1 shows a schematic layout of the planar waveguide-coupled square μ-cavity channel add-drop filter. A square μ-cavity of sidewall length *a* is laterally coupled with two parallel singlemode waveguides of width *w*. The cavity sidewall and the waveguide sidewall are separated with an air-gap distance g. In order to simulate the refractive index contrast between silicon and air, both singlemode waveguides and square μ-cavity have a refractive index n = 3.5 while the background refractive index is 1. The singlemode waveguide mode

#3001 - $15.00 US Received September 04, 2003; Revised October 24, 2003

has a propagation constant β, a discrete transverse k-vector component κ, and a mode angle $\phi = \tan^{-1}(\beta/\kappa)$. The waveguide mode k-vector is denoted as $\mathbf{k_{wg}}$.

Resonances of the high refractive-index contrast square cavity can be approximated by k-space modes, assuming the cavity field amplitude drops to zero at the cavity sidewall [7,8]. The **k**-vector (k_x, k_y) in the square cavity can be discretized as $k_x = m_x\pi/a$ and $k_y = m_y\pi/a$ with $(nk)^2 = k_x^2 + k_y^2$, where m_x and m_y are integers, and k is the vacuum propagation constant [7]. We denote the square cavity modes as (m_x, m_y). We can calculate the vacuum resonant wavelength $\lambda = 2na / (m_x^2 + m_y^2)^{1/2}$ and the corresponding mode angle $\theta = \tan^{-1}(m_y/m_x)$ [7]. For modes that have 4-bounce ray orbits, the TIR confinement requires $\theta_c < \theta < 90^o-\theta_c$ [7], where θ_c is the TIR critical angle. It has been recognized that (m_x, m_y) and (m_y, m_x) modes have the same λ, and thus (m_x, m_y) and (m_y, m_x) modes are degenerate, while they have θ and $90^o-\theta$ mode angles [7]. We define the mode number $M = m_x + m_y$. Modes with the same M values have the same integer number of wavelengths in wavefront-matched round-trip path lengths [7].

2.2 k-space mode field patterns

The mode field pattern of a (m_x, m_y) mode can be given as follows,

$$E_{mx,my}(x, y)\, e^{i\omega t} = A\, e^{i\omega t} \sin(m_x\pi x/a) \sin(m_y\pi y/a), \quad (1)$$

where we have chosen the origin at a square cavity corner (Fig. 1), ω is the mode angular frequency, and A is the field amplitude. Here, we consider only the electric field polarization in the z direction (out-of-plane), and therefore the field is essentially scalar in a 2-D plane. The mode field pattern is a 2-D standing wave along both the x and y directions, with m_x the number of field extrema along the x direction and m_y the number of field extrema along the y direction. Since (m_x, m_y) and (m_y, m_x) modes are degenerate, the resonant field pattern at wavelength λ at (m_x, m_y) mode (or λ at (m_y, m_x) mode) can be considered as the superposition of the degenerate pairs (neglecting other accidental degeneracy) as follows,

$$E_{mx,my}(x, y)\, e^{i\omega t} = A\, e^{i\omega t} \sin(m_x\pi x/a) \sin(m_y\pi y/a) + B\, e^{i(\omega t-\delta)} \sin(m_y\pi x/a) \sin(m_x\pi y/a), \quad (2)$$

where B is the amplitude of (m_y,m_x) mode, and δ is the relative phase between degenerate modes.

3. FDTD simulated spectra

We employed a commercially available 2-D FDTD photonic design tool [14] to simulate the device transmission characteristics. A 5.17-fs Gaussian pulse centered at vacuum wavelength 1.55 μm with fundamental slab waveguide mode profile was launched into the input port (Fig. 1). Spectral responses of the filter were obtained from the throughput, drop and add ports. We adopted a 15-nm spatial grid-size and a 0.02-fs temporal step. The spectral resolution was ≈ 0.08 nm – 0.16 nm. A perfectly matched layer (PML) of reflectivity 10^{-8} with a thickness of 1.5 μm in the y direction and of 0.5 μm in the x direction was used to absorb stray field at the simulation window boundaries. Mode field patterns were obtained by launching a continuous-wave (CW) at resonant wavelengths.

Figure 2 shows the FDTD simulated throughput (blue), drop (green) and add (red dashed line) spectra of a planar waveguide-coupled square μ-cavity filter with a = 2.2 μm, w = 0.2 μm and g = 0.2 μm. The polarization is TM (E-field ⊥ the plane). By choosing a to be 2.2 μm, we limit the number of modes in the multimode square μ–cavity [6,10,11]. It is entirely feasible to fabricate square μ–cavities of this size using standard photolithography. Multimode resonances are clearly discerned from the spectra. The resonance at λ = 1446.5 nm (denoted as $(7,9)_\pi$ mode) has the highest Q ≈ 1,600 and a coupling efficiency ≈ 74%.

#3001 - $15.00 US Received September 04, 2003; Revised October 24, 2003

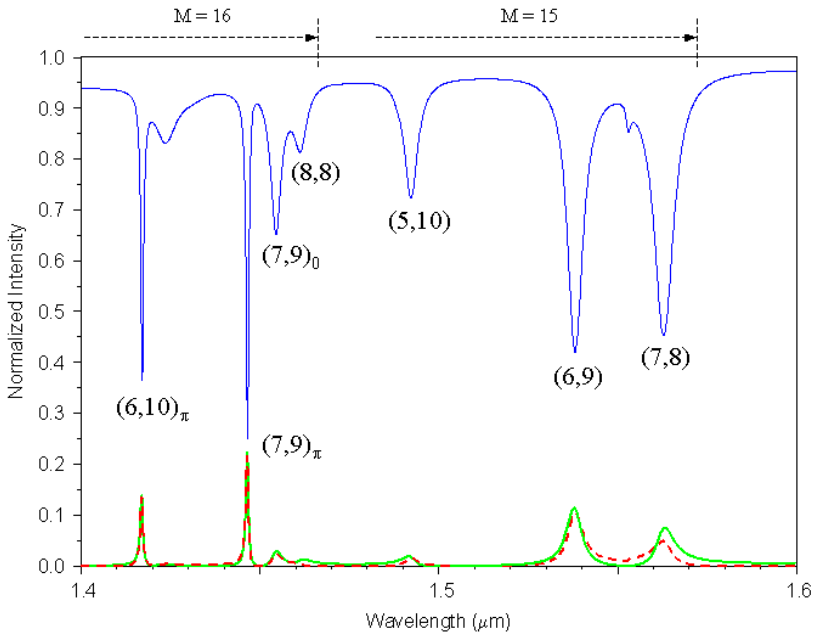

Fig. 2. FDTD simulated throughput (blue), drop (green) and add (red dashed line) spectra (normalized with input intensity) of a planar waveguide-coupled square μ–cavity filter. a = 2.2 μm, w = 0.2 μm, g = 0.2 μm and TM-polarized. The dominant resonances in the throughput spectrum are indexed as (m_x, m_y) modes according to the corresponding mode-field patterns. The indexed (m_x, m_y) modes are clustered according to the integer number of wavelengths M.

In order to identify the simulated resonances as (m_x, m_y) modes, we simulated their mode field patterns with time evolution. Either by counting the number of extrema along the x and y directions of the simulated mode field patterns or by comparing the simulated field patterns to the calculated mode field patterns using Eq. (2), we labeled the resonances by (m_x, m_y) the mode numbers and δ the relative phase between the degenerate modes. When one of the degenerate modes is preferentially coupled, we label the resonance by the dominant (m_x, m_y) mode. When the degenerate pairs are similarly coupled, we label the resonance by $(m_x, m_y)_\delta$, where the subscript denotes the estimated relative phase δ. Figure 2 depicts the (m_x, m_y) mode numbers for all the dominant resonances.

4. Resonant field patterns

4.1 Odd M resonances

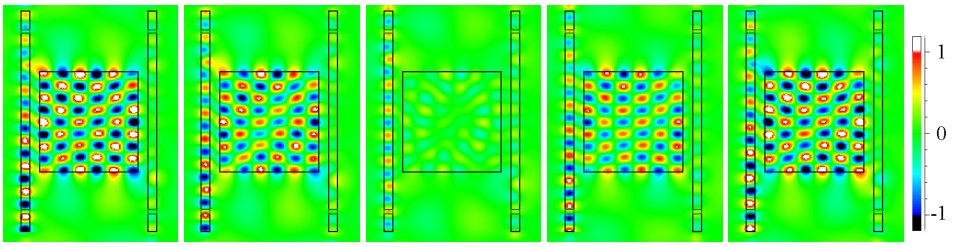

Fig. 3. FDTD simulated odd M (=15) mode field patterns of a planar waveguide-coupled square μ-cavity filter at (6,9) mode (λ = 1538 nm). a = 2.2 μm, w = 0.2 μm, g = 0.2 μm and TM-polarized. (a) $t = t_0$, (b) $t \approx t_0+T/8$, (c) $t \approx t_0+T/4$, (d) $t \approx t_0+3T/8$ and (e) $t \approx t_0+T/2$.

#3001 - $15.00 US
Received September 04, 2003; Revised October 24, 2003

Modes of different parity (odd or even) of M turn out to have distinctly different mode field patterns and spectral characteristics. Figures 3(a) – (e) show an example of the simulated odd M (=15) mode field patterns at λ = 1538 nm ((6,9) mode), evolving in time t within approximately a half period T/2, where $T \approx \lambda/c$, and c is the vacuum speed of light. The approximation in t and T is only limited by the simulation frame rate. Figure 3(a) shows the mode field pattern at an arbitrary initial time $t = t_o$. There exists 6 field extrema along the x direction and 9 field extrema along the y direction. Figures 3(b) – (e) show the mode field patterns at $t \approx t_o + T/8$, T/4, 3T/8, and T/2. The mode field pattern evolves as a 2-D standing wave and varies only in field amplitude. The mode field patterns enable us to identify this resonance as (6,9) mode.

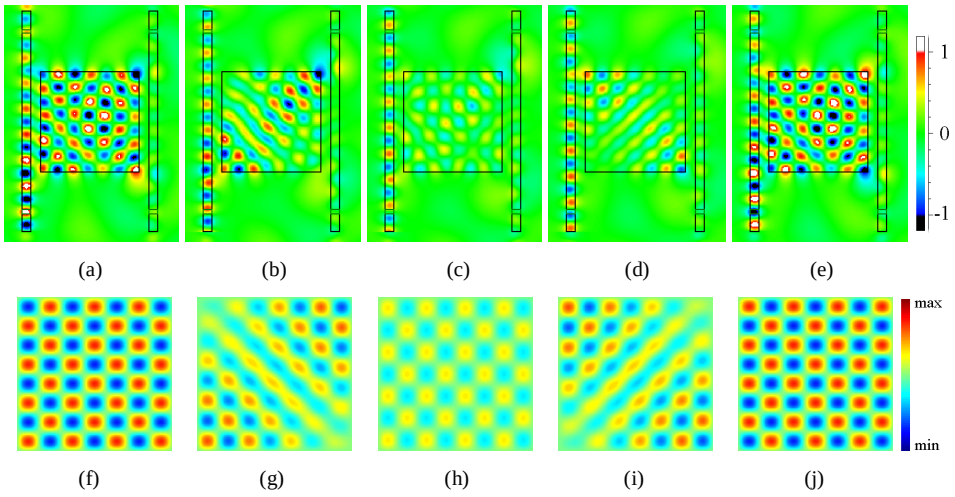

Fig. 4. FDTD simulated odd M (=15) mode field patterns of a planar waveguide-coupled square μ-cavity filter at (7,8) mode (λ = 1562.5 nm). *a* = 2.2 μm, *w* = 0.2 μm, *g* = 0.2 μm and TM-polarized. (a) $t = t_0$, (b) $t \approx t_0 + T/6$, (c) $t \approx t_0 + T/4$, (d) $t \approx t_0 + 2T/6$ and (e) $t \approx t_0 + T/2$. Calculated mode field patterns of a discrete square cavity using Eq. (2) with A = 0.7 for (7,8) mode, B = 0.3 for (8,7) mode, and $\delta = \pi/2$. (f) $\omega t = 0$, (g) $\omega t = 2\pi/6$, (h) $\omega t = \pi/2$, (i) $\omega t = 4\pi/6$ and (j) $\omega t = \pi$.

Figures 4(a) – (e) illustrate another set of simulated odd M (=15) mode field patterns at 1562.5 nm, evolving in time t within approximately a half period T/2. Figure 4(a) shows the mode field pattern at an arbitrary initial time $t = t_o$. There exists 7 field extrema along the x direction and 8 field extrema along the y direction. We identify this as (7,8) mode. Interestingly, at $t \approx t_0 + T/4$ (Fig. 4(c)), the mode field pattern appears as a weak field pattern with 8 field extrema along the x direction and 7 field extrema along the y direction. This suggests the co-existence of the degenerate (8, 7) mode with an estimated relative phase $\delta \approx \pi/2$.

At $t \approx t_0 + T/2$ (Fig. 4(e)), the mode field pattern returns to a pronounced (7,8) mode with approximately π phase difference from that at $t = t_0$ (Fig. 4(a)). Figures 4(b) and (d) show the mode field patterns at $t \approx t_0 + T/6$ and $t \approx t_0 + 2T/6$. It is evident that the preferentially coupled (7,8) mode and the degenerate (8,7) mode interfere with each other. The result is a superposition of standing waves that appears to oscillate between each degenerate mode. Figures 4 (f) – (j) show the calculated mode field patterns of a discrete square cavity using Eq. (2), with A = 0.7 for (7,8) mode, B = 0.3 for (8,7) mode and $\delta = \pi/2$, at ωt = (f) 0, (g) $2\pi/6$, (h) $\pi/2$, (i) $4\pi/6$, and (j) π. We find a good agreement between the simulated and calculated mode field patterns. Hence, we labeled the resonance by its dominant (7,8) mode. Similarly, we identified (5,10) modes at 1492.2 nm.

#3001 - $15.00 US Received September 04, 2003; Revised October 24, 2003

We remark that all (6,9), (7,8) and (5,10) modes (odd M) display field extrema at the square μ-cavity corners, as shown in Figs. 3 and 4, and thus the modes can be leaky at the sharp cavity corners. This is consistent with the simulated spectra (Fig. 2) that these modes have relatively low Q values (≈ 300).

4.2 Even M resonances

4.2.1 Vortex field patterns

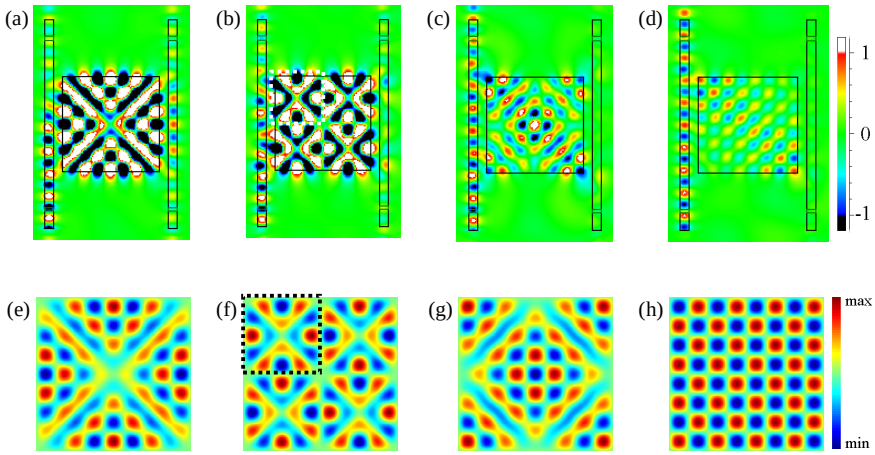

Fig. 5. FDTD simulated even M (=16) mode field patterns of a planar waveguide-coupled square μ-cavity filter. a = 2.2 μm, w = 0.2 μm, g = 0.2 μm and TM-polarized. (a) $(7,9)_\pi$ mode (λ = 1446.5 nm), (b) $(6,10)_\pi$ mode (λ = 1417.1 nm), (c) $(7,9)_0$ mode (λ = 1454.5 nm) and (d) (8,8) mode (λ = 1461.2 nm). Calculated mode field patterns of a discrete square cavity using Eq. (2) with A = B. (e) $(7,9)_\pi$ mode, (f) $(6,10)_\pi$ mode, (g) $(7,9)_0$ mode and (h) (8,8) mode. The dashed-line box in (b) and (f) denotes a "vortex."

For even M modes, we observe that the (m_x, m_y) and (m_y, m_x) degenerate pairs tend to interfere with $\delta \approx \pi$ or 0 with A ≈ B. Figures 5(a) and (b) show examples of the simulated even M (=16) mode field patterns at λ = 1446.5 nm and λ = 1417.1 nm. We have not shown the time evolution because these patterns evolve in time approximately as standing waves and only the field amplitude varies. By matching Figs. 5(a) and (b) with patterns obtained from Eq. (2), we identified these two resonances as $(7,9)_\pi$ and $(6,10)_\pi$. Figures 5(e) and (f) show the calculated mode field patterns of $(7,9)_\pi$ and $(6,10)_\pi$ of a discrete square cavity, using Eq. (2) with A = B and $\delta = \pi$. The calculations demonstrate an excellent agreement with the simulated patterns.

Figure 5(a) depicts a characteristic zero field amplitude at the cavity center that is surrounded by cross-like wavefronts [6,10-13]. We denote this characteristic mode field pattern as a "vortex." The number of vortices appears in an even M mode depends on $|m_x-m_y|$. Figure 5(a) shows one vortex with $|m_x-m_y| = 2$. Figure 5(b) shows five vortices (denoted by the dashed-line box) with $|m_x-m_y| = 4$. We found more complex arrangement of vortices (not shown) at modes with $|m_x-m_y| = 6$.

We remark that the even-M $(m_x, m_y)_\pi$ mode field patterns have zero field amplitude at the square cavity corners, as exemplified in Figs. 5(a) and (b). Thus, the cavity corner leakage problem can be alleviated, which permits relatively high Q values (>1000), as shown in Fig. 2.

#3001 - $15.00 US Received September 04, 2003; Revised October 24, 2003

4.2.2 0-π mode splitting

Figure 5(c) shows the simulated even M (=16) mode field pattern at λ = 1454.5 nm (denoted as $(7,9)_0$ mode). By comparing the simulated mode field pattern to the calculated mode field pattern, as shown in Fig. 5(g), we identified this mode as $(7,9)_0$ with A = B and $\delta = 0$. Based on the mode field time evolution (not shown here), $(7,9)_0$ mode field pattern is approximately a standing wave.

We remark that the even-M $(m_x, m_y)_0$ mode field pattern has field extrema at the square cavity corners, as exemplified in Fig. 5(c). Hence, the even-M $(m_x, m_y)_0$ modes can be leaky, and thus reduce the cavity Q. This is consistent with the observation that $(7,9)_0$ mode has a relatively low Q (as compared with $(7,9)_\pi$ mode), as shown in Fig. 2.

According to the k-space model, (7,9) and (9,7) modes should degenerate at the same wavelength. Surprisingly, the simulated even-M $(m_x, m_y)_0$ modes are red-shifted compared with the even-M $(m_x, m_y)_\pi$ modes (e.g., $(7,9)_0$ mode at $\lambda \approx$ 1454.5 nm and $(7,9)_\pi$ mode at $\lambda \approx$ 1446.5 nm), as shown in Fig. 2. We term this unexpected red-shift between $\delta \approx 0$ and $\delta \approx \pi$ even-M modes as "0-π mode splitting." We attribute the mode splitting to the fact that $\delta \approx 0$ modes have leaky field at the square cavity corners, and thus require an additional phase shift to satisfy the boundary condition at the cavity corners.

4.2.3 ($m_x = m_y$) modes

Figure 5(d) shows the simulated even M (=16) mode field pattern at λ = 1461.2 nm (denoted as (8,8) mode). There exists 8 field extrema along both the x and y directions. The mode field pattern evolves approximately as a standing wave. Therefore, we identify this to be (8,8) mode. Under the influence of the neighbor $(7,9)_0$ mode, the field amplitude along one diagonal is enhanced. Figure 5 (h) shows the calculated (8,8) mode field pattern.

For $m_x = m_y$ modes (e.g. (8,8) modes), the mode degenerate with itself (neglecting accidental degeneracy). The mode angle $\theta = 45^o$ corresponds to the closed ray orbits in a square cavity. Intuition based on ray optics suggests that $\theta = 45^o$ modes should be long-lived and high-Q because of the closed ray orbits. However, (8,8) modes do not have particularly high Q values or a large coupling efficiency, as shown in Fig. 2. This inconsistency between the ray optics intuition and the simulated spectrum can be partially attributed to the mode field patterns of ($m_x = m_y$) modes. ($m_x = m_y$) mode field patterns have mode field extrema at the cavity corners (Figs. 5 (d) and (h)), and thus ($m_x = m_y$) modes are leaky and can be low Q.

5. Waveguide preferential mode coupling

Figure 6 shows the calculated (m_x, m_y) modes of a discrete square cavity of a = 2.36 μm between spectral range λ = 1.4 μm and 1.6 μm. The y-axis is the mode angle θ. Only the modes that satisfy $\theta_c < \theta < 90^o - \theta_c$ are represented ($\theta_c \approx 16.6^o$ for n = 3.5). Each dot represents an (m_x, m_y) mode. The filled dots represent dominant modes identified from the simulated spectra (Fig. 2). In order to approximately account for TIR phase shifts at the waveguide-coupled square cavity sidewalls, k-space modes are calculated from a slightly larger square cavity. K-space mode wavelengths are in good agreement with FDTD simulated resonance wavelengths (Fig. 2). The modes of the same M values are distributed along various parabola curves [8]. The dashed line depicts the calculated slab waveguide (w = 0.2 μm) fundamental mode angle ϕ (Fig. 1) for various wavelengths in TM polarization [15].

When the lightwave is evanescently input side-coupled to the square μ-cavity, it is conceivable that the input-coupled wavefront should have a preferential spatial overlap and be coupled to (m_x, m_y) mode angle θ that is near ϕ. Consequently, cavity modes with θ in the neighborhood of ϕ can have a higher coupling efficiency and become dominant modes, while modes with θ farther from ϕ have a lower coupling efficiency.

#3001 - $15.00 US Received September 04, 2003; Revised October 24, 2003

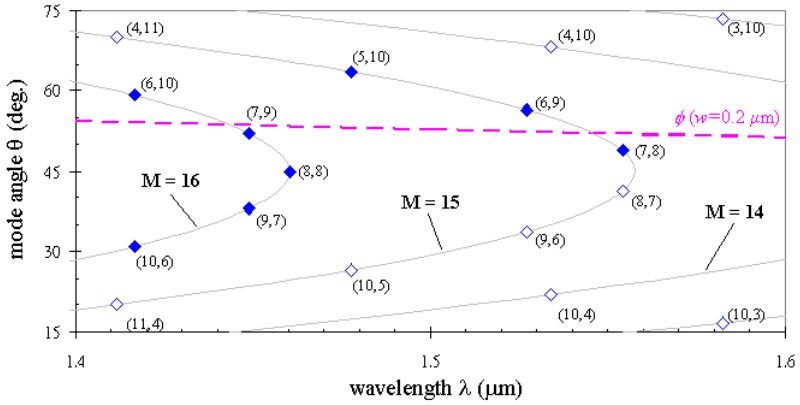

Fig. 6. Calculated k-space (m_x, m_y) modes (filled and open dots) of a discrete square cavity of a = 2.36 μm. The y-axis is the mode angle θ and the x-axis is the wavelength λ. Only the modes that satisfy $\theta_c < \theta < 90^o-\theta_c$ are represented ($\theta_c \approx 16.6^o$ for n = 3.5). The modes of the same M values are distributed along various parabola curves. The dominant modes in Fig. 2 are represented by filled dots. The dashed line shows the waveguide fundamental mode angle φ (w = 0.2 μm) in TM polarization.

It is generally valid that k-space modes that are closer to the waveguide mode (Fig. 6) have higher coupling efficiencies, as shown in Fig. 2. For example, (6,10), (7,9), (6,9) and (7,8) modes are the closest modes to the waveguide mode and have the highest coupling efficiencies among neighboring modes. In contrast, resonances (8,8) and (5,10) modes are farther from the waveguide mode and display a lower coupling efficiency.

For odd M modes, we observe that degenerate modes with θ ≈ φ are preferentially coupled over their degenerate partners. We observe from the simulated mode field patterns (Figs. 3 and 4) that (6,9), (7,8) and (5,10) modes are dominant over degenerate modes (9,6), (8,7) and (10,5). However, for even M modes, the preferential mode coupling can be modified and extended to the mode that has a degenerate partner close to the waveguide mode, e.g. (9,7) and (10, 6) modes are still significantly coupled when (7,9) and (6,10) modes are very close to the waveguide mode.

6. Conclusion

In summary, we have employed 2-D FDTD method to systematically study the mode field patterns and the mode coupling of a planar waveguide-coupled square μ-cavity channel add-drop filter. We demonstrated that the simulated resonances can be represented by k-space modes of a discrete square cavity. Resonant field patterns can be described by the interference of degenerate k-space modes. With different mode number parities, mode field patterns and spectral characteristics are distinctly different. We observe that cavity modes that have mode angles close to the waveguide mode angle are in general preferentially input coupled. However, the degree of preferential mode coupling can be modified by different mode number parities. We are currently fabricating planar waveguide-coupled square μ-cavity filters on silicon-based substrates to experimentally demonstrate some of the concepts discussed in this work [13]. Further numerical and analytical studies will focus on the distinction between different mode number parities.

Acknowledgment

This work was substantially supported by grants from the Research Grants Council and from the University Grants Council of the Hong Kong Special Administrative Region, China. (Project No. HKUST6166/02E and HIA01/02.EG05.)